Human Molecular Genetics, 2013, Vol. 22, No. 3 **452–465**
doi:10.1093/hmg/dds441
Advance Access published on October 16, 2012

Hip14l-deficient mice develop neuropathological and behavioural features of Huntington disease

Liza M. Sutton, Shaun S. Sanders, Stefanie L. Butland, Roshni R. Singaraja, Sonia Franciosi, Amber L. Southwell, Crystal N. Doty, Mandi E. Schmidt, Katherine K.N. Mui, Vlad Kovalik, Fiona B. Young, Weining Zhang and Michael R. Hayden*

Centre for Molecular Medicine and Therapeutics, University of British Columbia, Vancouver, British Columbia V5Z 4H4, Canada

Received August 24, 2012; Revised October 5, 2012; Accepted October 11, 2012

Palmitoylation, the dynamic post-translational addition of the lipid, palmitate, to proteins by Asp-His-His-Cys-containing palmitoyl acyltransferase (PAT) enzymes, modulates protein function and localization and plays a key role in the nervous system. Huntingtin-interacting protein 14 (HIP14), a well-characterized neuronal PAT, has been implicated in the pathogenesis of Huntington disease (HD), a fatal neurodegenerative disease associated with motor, psychiatric and cognitive symptoms, caused by a CAG expansion in the huntingtin gene (*HTT*). Mice deficient for *Hip14* expression develop neuropathological and behavioural features similar to HD, and the catalytic activity of HIP14 is impaired in HD mice, most likely due to the reduced interaction of HIP14 with HTT. Huntingtin-interacting protein 14-like (HIP14L) is a paralog of HIP14, with identical domain structure. Together, HIP14 and HIP14L are the major PATs for HTT. Here, we report the characterization of a *Hip14l*-deficient mouse model, which develops adult-onset, widespread and progressive neuropathology accompanied by early motor deficits in climbing, impaired motor learning and reduced palmitoylation of a novel HIP14L substrate: SNAP25. Although the phenotype resembles that of the *Hip14*$^{-/-}$ mice, a more progressive phenotype, similar to that of the YAC128 transgenic mouse model of HD, is observed. In addition, HIP14L interacts less with mutant HTT than the wild-type protein, suggesting that reduced HIP14L-dependent palmitoylation of neuronal substrates may contribute to the pathogenesis of HD. Thus, both HIP14 and HIP14L may be dysfunctional in the disease.

INTRODUCTION

Palmitoylation is the reversible post-translational addition of palmitate, a 16-carbon fatty acid, to proteins at cysteine residues via a thioester bond. Palmitoylation modulates protein function by influencing trafficking, membrane association, lipid raft localization, stability and protein–protein interaction. Palmitoylation is an essential post-translational modification for a diverse range of proteins and is the most frequent lipid modification of the nervous system, where it plays a key role in neuronal development, synaptic plasticity and synaptic localization (reviewed in 1). For example, palmitoylation localizes the gamma-amino butyric acid-synthesizing enzyme, glutamate decarboxylase (GAD65), to the presynaptic terminal for neurotransmitter release (2,3) and post-synaptic density-95 (PSD-95) to the excitatory post-synaptic terminal, where it acts as a scaffold for α-amino-3-hydroxy-5-methyl-4-isoxazolepropionic acid (AMPA) and *N*-methyl-D-aspartate (NMDA) receptors and regulates activity-dependent plasticity (4–6). Given the importance of palmitoylation in the nervous system, it is not surprising that aberrant palmitoylation has been associated with a number of neuropsychiatric diseases, including schizophrenia, mental retardation, Alzheimer's disease, infantile ceroid lipofuscinosis and Huntington disease (HD; 7–15).

HD is an adult-onset neurodegenerative disorder associated with motor disturbances, psychiatric symptoms and cognitive decline (16). It is caused by a CAG repeat expansion of over 35 repeats in the *HTT* gene (17) that translates to a toxic polyglutamine expansion in the huntingtin (HTT) protein. Early striatal degeneration is the defining neuropathological hallmark of HD, but it is a disease affecting many brain regions (16). To study HD, we developed the YAC128 mouse model that contains the entire human *HTT* gene, including the upstream regulatory region, with 128 CAG repeats.

*To whom correspondence should be addressed. Tel: +1 6048753535; Fax: +1 6048753819; Email: mrh@cmmt.ubc.ca

The YAC128 mouse model recapitulates many neuropathological and behavioural features of HD, including striatal volume loss, enkephalin-expressing medium spiny neuron (MSN) loss in the striatum and motor and cognitive dysfunction (18).

Palmitoylation is mediated by palmitoyl acyltransferases (PAT), a class of enzymes that possess a signature cysteine-rich, DHHC-containing catalytic domain (DHHC-CR; 19,20). There are 23 mammalian PATs with distinct but overlapping substrate specificities (19,21,22). HIP14 was the first identified mammalian PAT and regulates the palmitoylation and trafficking of several synaptic proteins, including HTT, SNAP25, GAD65, PSD-95 and synaptotagmin I (23,24). Several lines of evidence point to the involvement of HIP14 in the pathogenesis of HD. The interaction between HTT and HIP14 is reduced in the presence of the HD mutation and not only is HTT a substrate for HIP14 but wild-type HTT (but not mutant HTT) enhances HIP14 PAT activity (11,25). Loss of *Hip14* expression in mice results in the development of early-onset striatal degeneration and deficits in motor coordination and neuronal palmitoylation that are reminiscent of features of HD (11). HIP14 is dysfunctional in YAC128 mice, likely due to its reduced interaction with HTT and its altered localization (11). Taken together, these data point to aberrant palmitoylation of neuronal substrates as a potential mechanism contributing to the pathogenesis of HD.

Huntingtin-interacting protein 14-like (HIP14L or ZDHHC13) was identified in a database search for *HIP14* homologs but has not been well characterized (24). HIP14L shares identical domain structure and 57% sequence similarity with HIP14 in humans (7,24), and these two PATs are the major PATs for HTT *in vitro* (25). HIP14L is ubiquitously expressed, and one reported mutation of the *Hip14l* gene results in a wide range of physiological disturbances in mice (26). The mice, in which a nonsense mutation was introduced into exon 12 of the *Hip4l* gene ($Hip14l^{R425X}$) by *N*-ethyl-*N*-nitrosourea mutagenesis and truncated HIP14L before the catalytic domain, exhibited severe phenotypes, including shortened life span (20% survival at 12 months), 50% reduced body weight at all ages, skin and hair abnormalities, including alopecia, bone abnormalities, including osteoporosis and kyphosis and systemic amyloidosis. However, the consequences of the $Hip14l^{R425X}$ mutation in the CNS were not formally explored.

To determine the function of HIP14L in the CNS and whether HIP14L plays a role in HD, we generated and characterized a *Hip14l*-deficient mouse model ($Hip14l^{-/-}$). The mice develop adult-onset, widespread and progressive neuropathological deficits, accompanied by motor impairment, motor learning deficits and reduced palmitoylation of SNAP25. $Hip14l^{-/-}$ mice resemble those with *Hip14* deficiency, but develop an adult-onset, progressive phenotype more consistent with that seen in HD.

RESULTS

HIP14L and HIP14 share identical domain structure and a high degree of amino acid similarity in their functional domains

HIP14 and HIP14L are more closely related to each other than to any of the other mammalian PATs. The domain structure of HIP14L and HIP14 is identical, with an ankyrin domain, six transmembrane domains (TM1–6) and the signature PAT DHHC-CR catalytic domain (22; Fig. 1). Recently, homology modelling, using the crystal structure of the N-terminus of HIP14, revealed that both PATs contain seven ankyrin repeats within the ankyrin domain, a region that distinguishes them from the other PATs and mediates protein–protein interactions (7). The DHHC-CR domain lies between TM4 and TM5. HIP14L is unique among mammalian PATs because it contains a DQHC sequence within the DHHC-CR domain, as opposed to the canonical DHHC motif. This is unlikely to impair its PAT activity because it has been shown to palmitoylate HTT, GAD65, IgG kappa light chain and Gp78 *in vitro* (25–27).

Pairwise sequence alignment of the mouse HIP14L and HIP14 proteins indicates that they share 63% sequence similarity and 46% sequence identity. A conservation plot of these two sequences illustrates that they are most similar at the N-terminal ankyrin domain (ANK1-ANK3) and in the DHHC-CR catalytic domain, consistent with their role in catalysis (Fig. 1B).

Interaction of HIP14L with HTT is reduced in the presence of the HD mutation

Because HIP14L is a major PAT for HTT (25) and has identical domain structure to HIP14, we hypothesized that, like HIP14, HIP14L may also be a HTT-interacting protein. Co-immunoprecipitation (co-IP) assays were performed following overexpression of HIP14L and an N-terminal fragment of HTT (N548-HTT) in COS cells. HIP14L interacted with wild-type 15Q HTT, but significantly less with mutant 128Q HTT, confirming HIP14L as an HTT interactor which may play a role in the pathogenesis of HD (Fig. 2). Consistent with previous observations, HIP14 also interacted less robustly with mutant HTT (24).

Expression of *Hip14l* in mouse tissues

The normal tissue distribution of *Hip14l* in wild-type mice was determined by a quantitative RT-PCR (qRT-PCR) assay using primers located in exons 4 and 5. Due to the absence of a reliable antibody for HIP14L, protein levels were not assessed. In adult wild-type mice at 3 months, *Hip14l* mRNA expression was detected in whole brain, in all peripheral tissues tested (heart, muscle, kidney, spleen, liver and lung; Fig. 3A) and in all brain regions tested (Fig. 3B). This corroborates previous data in mice and humans, which indicate that *Hip14l* expression is ubiquitous (http://biogps.gnf.org; 26). The *Hip14l* mRNA expression pattern is similar to human *HIP14* mRNA, in that there is higher expression in the brain, heart, muscle and kidney than in the lung and liver (24).

Generation of $Hip14l^{-/-}$ mice

To determine the role of HIP14L in the CNS and to determine whether, like HIP14, it plays a role in the pathogenesis of HD, a *Hip14l*-deficient mouse ($Hip14l^{-/-}$) was generated. A gene trap strategy was employed, in which the gene trap vector was inserted into intron1 of *Hip14l* (Supplementary Material, Fig. S1). *Hip14l* gene trap transgenic mice were backcrossed from the 129/Ola strain to the FVB strain background

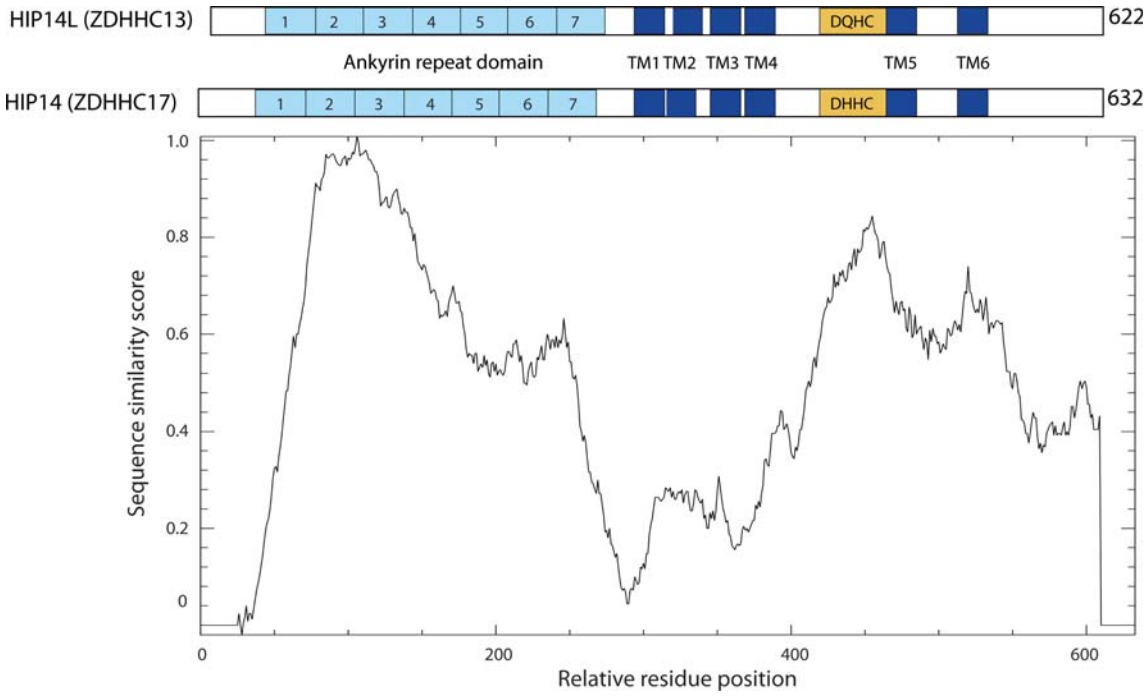

Figure 1. Comparison of HIP14L and HIP14 functional domains and amino acid sequence. HIP14L and HIP14 share an identical domain structure that includes an ankyrin repeat domain containing seven ankyrin repeats, six transmembrane domains (TM1–6) and a DHHC-CR catalytic domain (labelled DQHC and DHHC in HIP14L and HIP14, respectively). A conservation plot comparing mouse HIP14L (NP_082307.1) and HIP14 (NP_766142.2) amino acid sequences, using a sliding window of 50 amino acids, reveals the highest similarity in the N-terminal half of the ankyrin repeat domain and lower similarity in ankyrin repeats 4–7. The next highest similarity peak coincides with the DHHC-CR catalytic domain. Similarity score is described in the Materials and Methods section. A conservation plot of mammalian HIP14L and HIP14 sequences from human (NP_061901.2, NP_056151.2), chimpanzee (XP_508324.2, XP_509231.2), dog (XP_854853.1, XP_539691.2) and mouse (NP_082307.1, NP_766142.1) yielded an essentially identical plot (data not shown).

(to N5) to allow comparison to both the *Hip14*$^{-/-}$ mice and YAC128 mice on the same background (11,18).

The *Hip14l*$^{-/-}$ mice were analyzed with the same qRT-PCR assay described above, in which primers were located downstream of the gene trap vector insertion. *Hip14l* mRNA was found to be absent from brain, liver and kidney of *Hip14l*$^{-/-}$ mice when compared with wild-type littermate controls, confirming that the gene trap completely abolished *Hip14l* mRNA expression (Fig. 3C).

Hip14l$^{-/-}$ mice are viable and fertile and, unlike the *Hip14l*^{R425X} mice, did not differ in their survival at 12 months of age when compared with wild-type littermate controls (data not shown). There was a trend towards reduced body weight of the *Hip14l*$^{-/-}$ mice, which weighed progressively less from 3 to 12 months [repeated measures ANOVA (RMA) genotype: $P = 0.074$, age: $P < 0.0001$, interaction: $P < 0.0001$; Fig. 6G]. *Hip14l*$^{-/-}$ mice displayed hypotrichosis (reduced hair growth) and alopecia (absence of hair) around the eyes (Supplementary Material, Fig. S2A). Dorsal skin was assessed at post-natal day 7, when the hair follicles reach full maturity (28). At this stage, *Hip14l*$^{-/-}$ mice exhibited a 26% reduction in hair follicle density when compared with wild-type controls ($P = 0.017$; Supplementary Material, Fig. S2B). In contrast to the *Hip14l*^{R425X} mice, thickening of the epidermis, absence of hair shafts in follicles and reduction in the adipose tissue were not detected in *Hip14l*$^{-/-}$ skin. No further abnormalities were observed by necropsy examination of the skeleton and peripheral organs, including amyloid deposition (data not shown).

Hip14l$^{-/-}$ mice exhibit progressive neuropathological deficits and HD-like striatal pathology

Because *Hip14*$^{-/-}$ mice display developmental neuropathology, we assessed brain and cerebellar weights of *Hip14l*$^{-/-}$ mice, beginning at 1 month of age. No difference in brain and cerebellar weights of *Hip14l*$^{-/-}$ mice was observed at 1 month when compared with wild-type littermates. Longitudinal analysis of brain and cerebellar weights from 1 to 12 months revealed a highly significant effect of genotype and age on the two measures (brain: two-way ANOVA genotype: $P < 0.0001$, age: $P < 0.0001$; interaction: $P = 0.063$; cerebellum: two-way ANOVA genotype: $P < 0.0001$, age: $P < 0.0001$; interaction: $P = 0.99$; Fig. 4A and B). Brain and cerebellar weights of *Hip14l*$^{-/-}$ mice were reduced in adulthood from 3 months (4.8% for brain weight and 6.2% for cerebellar weight) to 12 months of age (9.1% for brain weight and 6.4% for cerebellar weight). A trend towards a significant interaction of age and genotype for brain weight indicates that the loss in brain weight in the *Hip14l*$^{-/-}$ mice is likely to be progressive.

The brain regions classically associated with HD pathology are the striatum and cortex. Stereological assessment of the striatum and cortex in the *Hip14l*$^{-/-}$ mice revealed a pattern that was similar to the changes observed for brain weight. No difference was observed in the striatal and cortical volumes of *Hip14l*$^{-/-}$ mice at 1 month of age when compared with wild-type littermates, and striatal and cortical volumes

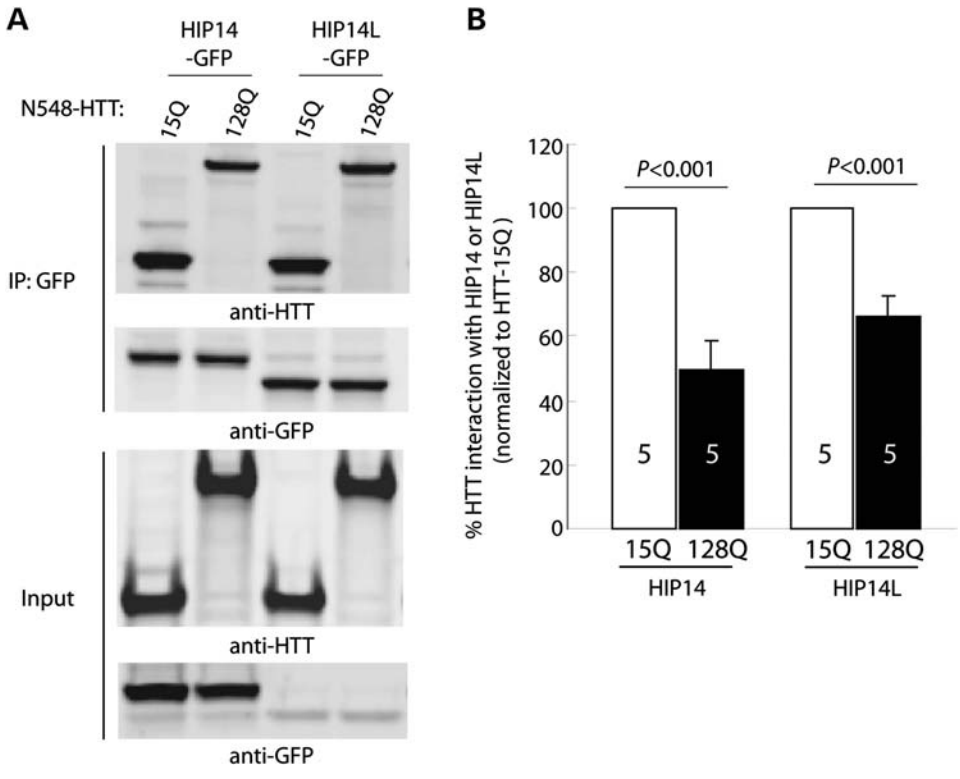

Figure 2. Interaction of HIP14L and HIP14 with HTT is inversely proportional to polyglutamine tract length. (A) Co-IP of either HIP14-GFP or HIP14L-GFP with wild-type HTT (N548-HTT 15Q) and mutant HTT (N548-HTT 128Q) in COS-7 cells. Reduced interaction of both HIP14L and HIP14 with N548-HTT 128Q was detected when compared with N548-HTT 15Q. The lower part of (**A**) shows HTT and HIP14- and HIP14L-GFP expression in 20 μg protein lysate; expression of HIP14L was considerably lower than that of HIP14. As HIP14L is expressed at a lower level in transfected COS-7 cells, to equalize the amount of HIP14 and HIP14L immunoprecipitated, 1500 μg of HIP14L lysate and 200 μg of HIP14 lysate were used for input to the IPs. (**B**) Quantification of co-IP experiments: HTT pull down was quantified relative to HIP14 or HIP14L pulldown and subsequently normalized to N548-HTT 15Q pull down. Data from five independent experiments indicated a significant reduction in the interaction of both HIP14 and HIP14L with N548-HTT 128Q relative to N548-HTT 15Q ($P < 0.001$); error bars represent mean + SEM and data were analyzed by Student's t-test. $n = 5$.

were progressively reduced from 3 months of age (5.7% for striatal volume and 8.4% for cortical volume) to 12 months of age (9.8% for striatal volume and 8.3% for cortical volume; striatum: two-way ANOVA genotype: $P < 0.0001$, age: $P = 0.072$; interaction: $P = 0.0005$; cortex: two-way ANOVA genotype: $P < 0.0001$, age: $P = 0.0093$; interaction: $P = 0.0040$; Fig. 4C and E). Striatal neuronal count was reduced by 15.8% ($P = 0.0028$) in the *Hip14l*$^{-/-}$ mice at 6 months of age, indicating that the striatal volume loss was due to neuronal cell death (Fig. 4D).

HD affects other regions of the brain in addition to the striatum and cortex (16). A recent study shows the most discriminatory brain regions in the YAC128 HD mouse model when compared with wild-type mice included subcortical grey matter regions and white matter regions that were reduced in volume, whereas hippocampus was reliably unchanged (29). Consequently, we performed stereological assessment of the globus pallidus, thalamus, corpus callosum and hippocampus in the *Hip14l*$^{-/-}$ mice. In the *Hip14*$^{-/-}$ mice, all these structures are reduced in volume (11). Female *Hip14l*$^{-/-}$ mice were studied because no significant difference was found between genders in previously analyzed neuropathological parameters. *Hip14l*$^{-/-}$ mice displayed a significant reduction in volume of the thalamus (two-way ANOVA genotype: $P = 0.0003$, age: $P = 0.38$; interaction: $P = 0.51$) and corpus callosum (two-way ANOVA genotype: $P < 0.0001$, age: $P < 0.0001$; interaction: $P = 0.32$) at 3 and 6 months and a significant reduction in volume of the globus pallidus at 6 months (two-way ANOVA genotype: $P = 0.05$, age: $P = 0.42$; interaction: $P = 0.044$). Hippocampal volumes remained unchanged at 3 and 6 months (two-way ANOVA genotype: $P < 0.34$, age: $P = 0.045$; interaction: $P = 0.76$; Fig. 4F–I).

In HD, the most severely affected striatal neuronal population is the met-enkephalin/dopamine receptor-2-expressing MSNs of the indirect pathway, whereas the substance P/DR1-expressing MSNs of the direct pathway remain largely unaffected until late stages of the disease (30). Striatal neurochemistry was assessed in the *Hip14l*$^{-/-}$ mice at 6 months of age. Dopamine- and cAMP-regulated phosphoprotein of M_r 32 000 (DARPP-32), which is a marker of the GABAergic MSNs that comprise 90% of the striatum, was reduced by 32% in the *Hip14l*$^{-/-}$ striatum ($P = 0.048$). Enkephalin levels were reduced by 53% ($P = 0.012$; Fig. 5A–D, and substance P levels remained unchanged in the *Hip14l*$^{-/-}$ striatum ($P = 0.87$; Fig. 5E and F).

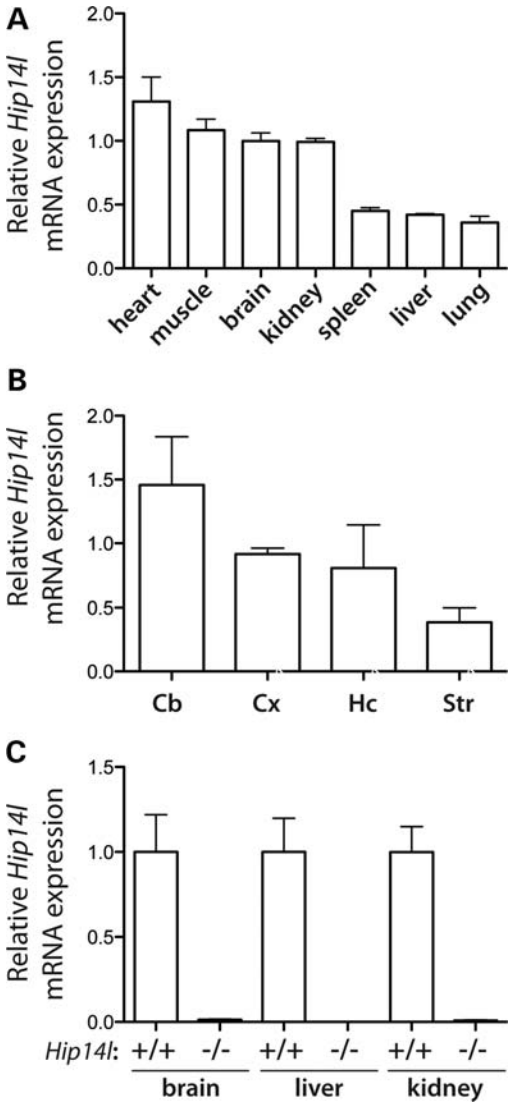

Figure 3. Normal tissue distribution of *Hip14l* in adult mice and loss of *Hip14l* expression in gene trap mice. *Hip14l* mRNA expression in (**A**) adult tissues and (**B**) brain regions at 3 months, as assessed by qRT-PCR (Cb = cerebellum; Cx = cortex; Hc = hippocampus; Str = striatum). Expression was calculated relative to β-actin ($n = 3$). (**C**) Absence of *Hip14l* mRNA in brain, liver and kidney of *Hip14l* gene trap (−/−) mice when compared with wild-type mice (+/+) by qRT-PCR at 3 months of age. Expression was calculated relative to β-actin ($n = 3$).

Hip14l$^{-/-}$ mice are hypoactive, display motor learning deficits and motor impairment

To determine whether the significant widespread CNS pathology observed in *Hip14l*$^{-/-}$ mice was associated with behavioural changes, the mice were subjected longitudinally to a number of motor and cognitive tasks. Spontaneous locomotor activity was assessed at 3, 6 and 12 months of age. *Hip14l*$^{-/-}$ mice were hypoactive when compared with wild-type mice from 3 to 12 months (Fig. 6A–D). RMA revealed a significant effect of genotype on the majority of parameters recorded: ambulatory time (RMA genotype: $P < 0.0001$, age: $P = 0.67$; interaction: $P = 0.98$), distance travelled (RMA genotype: $P < 0.0001$, age: $P = 0.21$; interaction: $P = 0.79$), resting time (RMA genotype: $P < 0.0001$, age: $P = 0.13$; interaction: $P = 0.062$) and vertical time (RMA genotype: $P < 0.0001$, age: $P = 0.95$; interaction: $P = 0.017$). No effect of genotype was observed for velocity (RMA genotype: $P = 0.30$, age: $P = 0.0047$; interaction: $P = 0.78$; data not shown).

Balance and motor coordination of *Hip14l*$^{-/-}$ mice were assessed on the accelerating rotarod task at 3–12 months. Initially, mice were trained on a fixed speed rotarod for 3 days. RMA revealed a trend towards a significant effect of genotype on rotarod training (RMA genotype: $P = 0.070$, trial: $P < 0.0001$; interaction: $P = 0.21$). The *Hip14l*$^{-/-}$ mice spent significantly less time on the rotarod on Day 1 when compared with wild-type mice, according to the *post hoc* analysis (Fig. 6E), indicating that the *Hip14l*$^{-/-}$ mice have a motor learning impairment. On the accelerating rotarod task, the performance of *Hip14l*$^{-/-}$ mice did not differ significantly from that of the wild-type controls indicating no obvious impairment of motor coordination (RMA genotype: $P = 0.45$, age: $P < 0.0001$; interaction: $P = 0.63$; Fig. 6F). To further investigate motor coordination in the *Hip14l*$^{-/-}$ mice, they were subjected to a climbing task. At 2 months of age, *Hip14l*$^{-/-}$ mice performed 65% fewer climbing events ($P = 0.0004$) and spent 41% less time climbing ($P = 0.065$; data not shown) than wild-type controls (Fig. 6H). *Hip14l*$^{-/-}$ mice showed no difference in the number of rearing events ($P = 0.92$) or time taken to start climbing ($P = 0.80$; data not shown), indicating that reduced climbing in *Hip14l*$^{-/-}$ mice was not the result of reduced motivation to climb.

Palmitoylation of neuronal substrate, SNAP25, is reduced in *Hip14l*$^{-/-}$ mice

To determine whether the loss of *Hip14l* results in the loss of palmitoylation of proteins in the brain, we assessed the palmitoylation status of selected neuronal substrates, including HTT and those that were reduced in the *Hip14*$^{-/-}$ mice: PSD-95 and synaptosomal-associated protein-25 (SNAP25). Although HTT is a HIP14L substrate *in vitro*, HTT palmitoylation was unchanged in *Hip14l*$^{-/-}$ brain ($P = 0.13$, Fig. 7A and B). Because HIP14 and HIP14L are the predominant PATs for HTT, it is likely that HIP14 is compensating for the loss of HIP14L in *Hip14l*$^{-/-}$ brain to palmitoylate HTT. Consistent with *in vitro* data, PSD-95 palmitoylation was unchanged in *Hip14l*$^{-/-}$ brain when compared with wild type, indicating that HIP14 and HIP14L have some different substrates ($P = 0.28$, Fig. 7C and D; 11). Interestingly, there was a 33% reduction in SNAP25 palmitoylation in *Hip14l*$^{-/-}$ brains ($P = 0.031$), indicating that SNAP25 is a HIP14L substrate *in vivo* (Fig. 7E and F).

DISCUSSION

In this study, we provide evidence that HIP14L is important in the CNS and its dysfunction may play a role in the pathogenesis of HD. We characterized regions of sequence similarity in the functional domains of HIP14L and HIP14, and we showed that, like HIP14, the interaction between HIP14L and mutant HTT is impaired. Loss of *Hip14l* expression *in vivo* led to the development of adult-onset, widespread and progressive

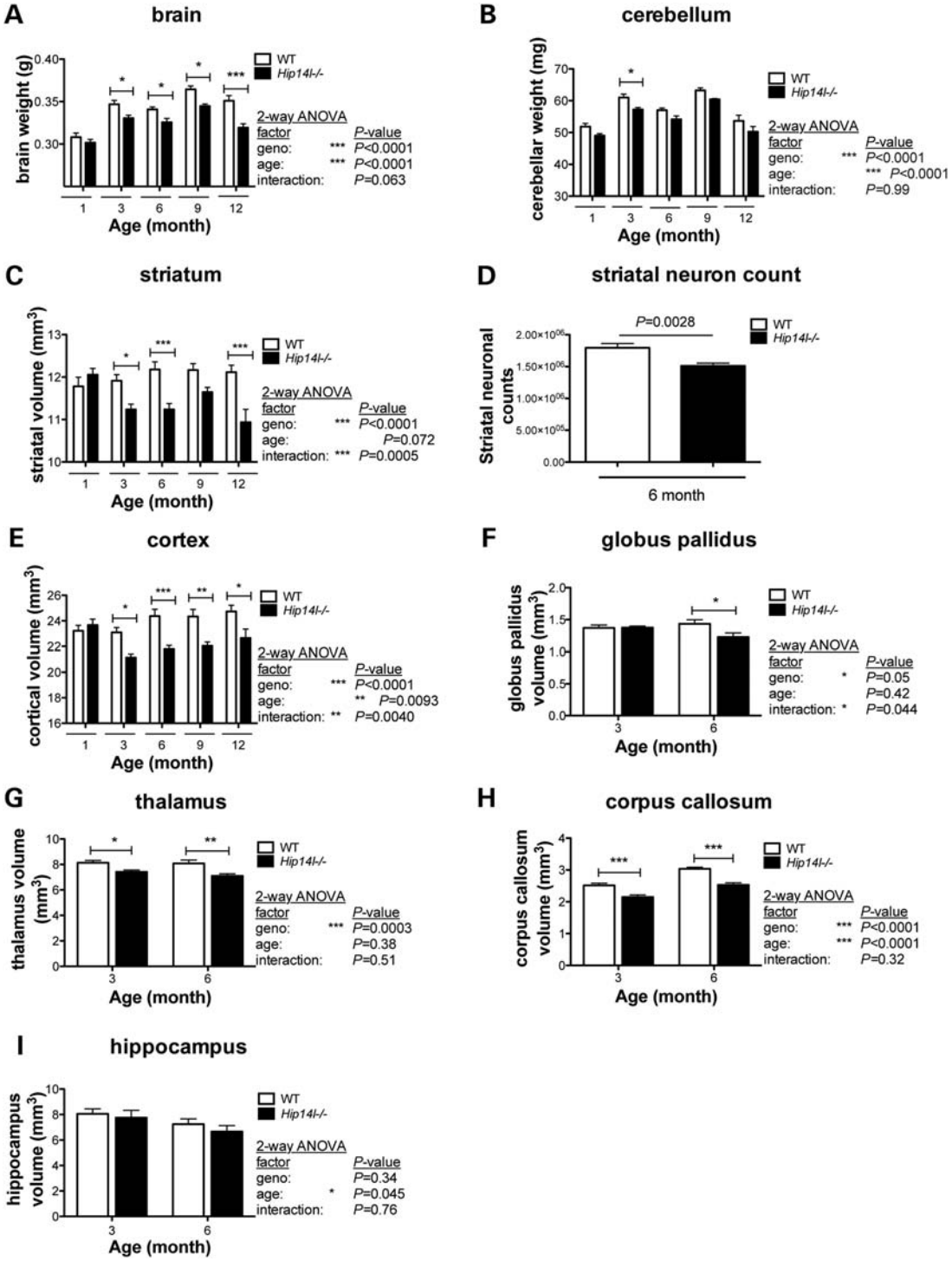

Figure 4. *Hip14l*$^{-/-}$ mice display post-natal widespread and progressive neuropathological deficits. (**A** and **B**) Brain and cerebellar weights of *Hip14l*$^{-/-}$ mice were unchanged from wild-type littermate controls at 1 month of age and were significantly reduced from 3 to 12 months relative to wild-type controls (WT). (**C** and **E**) Striatal and cortical volumes were unchanged in *Hip14l*$^{-/-}$ mice when compared with wild-type littermate controls at 1 month of age and were significantly and progressively reduced from 3 to 12 months relative to WT controls. $n = 1$ month: brain and cerebellar weights: 11 (WT), 10 (*Hip14l*$^{-/-}$); 1 month: striatal and cortical volumes: 16–17 (WT), 16–18 (*Hip14l*$^{-/-}$); 3 months: 16–17 (WT), 15–16 (*Hip14l*$^{-/-}$); 6 months: 15–18 (WT), 14–15 (*Hip14l*$^{-/-}$); 9 months: 13–15 (WT), 13–14 (*Hip14l*$^{-/-}$); 12 months: 15–17 (WT), 11–14 (*Hip14l*$^{-/-}$); mixed sex. Data were analyzed by two-way ANOVA. (**D**) Striatal neuronal count was reduced in *Hip14l*$^{-/-}$ mice by 15.8% at 6 months. $n = 5$ (WT), 8 (*Hip14l*$^{-/-}$). Data are represented as mean ± SEM and were analyzed by Student's *t*-test. *Hip14l*$^{-/-}$ mice displayed a significant reduction in volume of (**G**) thalamus, (**H**) corpus callosum at 3 and 6 months and of the (**F**) globus pallidus at 6 months. (**I**) Hippocampal volume remained unchanged at 3 months. $n = 3$ months: 9–10 (WT), 8–9 (*Hip14l*$^{-/-}$); $n = 6$ months: 8–9 (WT), 7–8 (*Hip14l*$^{-/-}$); females. All data are represented as mean ± SEM and were analyzed by two-way ANOVA. Significance of *t*-test or *post hoc* Bonferroni comparisons of genotype is indicated by *($P < 0.05$), **($P < 0.01$), ***($P < 0.001$).

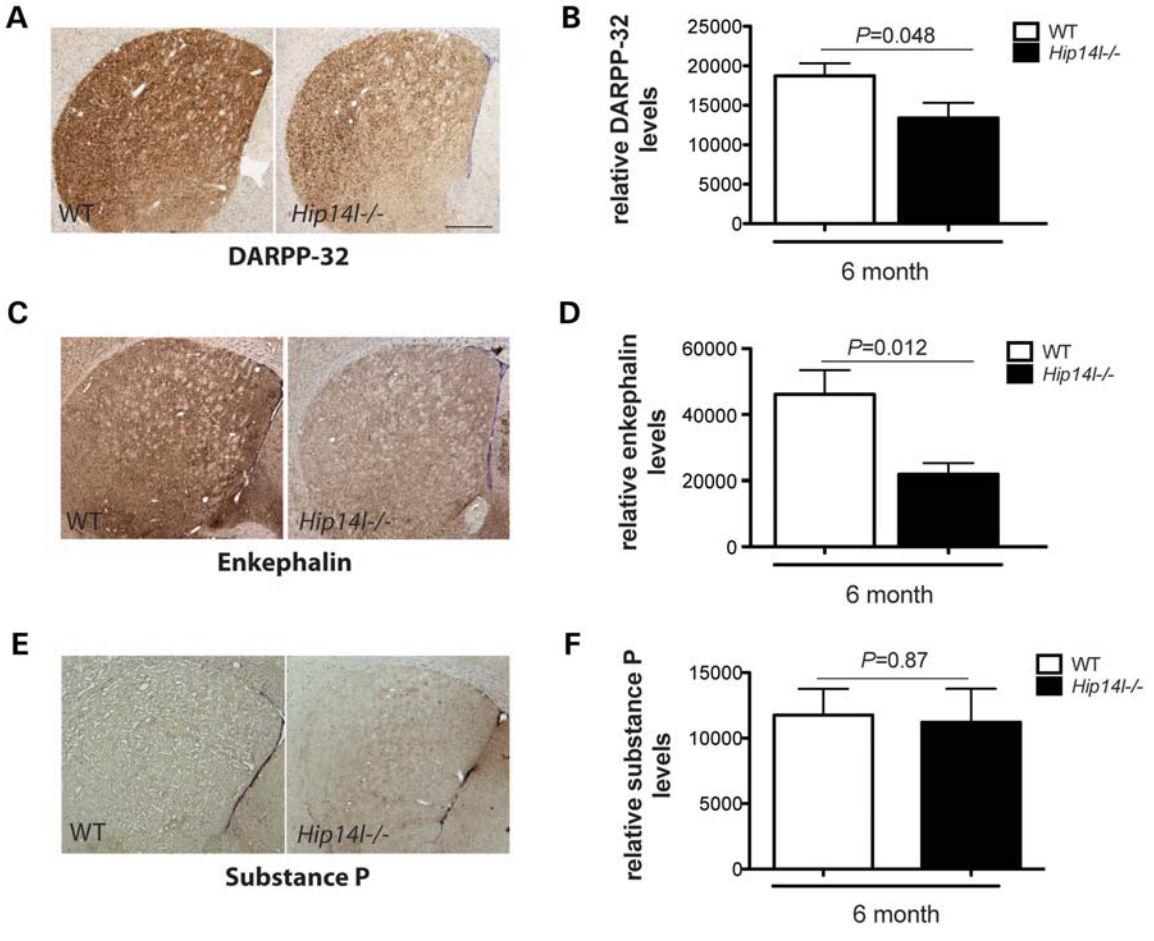

Figure 5. HD-like neurochemical changes in *Hip14l*$^{-/-}$ striatum. (**A** and **B**) DARPP-32 is a marker of MSNs. DARRP-32 levels were significantly reduced by 32% in the *Hip14l*$^{-/-}$ striatum at 6 months of age. (**C** and **D**) The met-enkephalin subpopulation of MSNs is affected in HD. Enkephalin levels were significantly reduced in *Hip14l*$^{-/-}$ striatum at 6 months by 53%. (**E** and **F**) The substance P-containing MSNs are unaffected in HD. Levels of substance P in the striatum of *Hip14l*$^{-/-}$ mice remained unchanged at 6 months. All bars represent means ± SEM, and data were analyzed by Student's *t*-test. $n = 5–9$ (WT), $n = 6–8$ (*Hip14l*$^{-/-}$); females.

neuropathology that was associated with early motor deficits in climbing, impaired motor learning and reduced palmitoylation of a novel HIP14L substrate: SNAP25. This phenotype is similar to the *Hip14*$^{-/-}$ mice and also resembles that of the YAC128 HD mice.

Comparison of *Hip14l*$^{-/-}$ and YAC128 HD mice

Hip14l$^{-/-}$ mice displayed a pattern and time course of neuropathology similar to the YAC128 mice (Table 1). Loss of brain volume and striatal volume occurs at 3 months of age, and both mice develop HD-like striatal neurochemical profiles by 6 months of age (18,29,30). Similar brain regions are affected in both mice: cortex, globus pallidus, thalamus and corpus callosum volumes are reduced and hippocampal volumes remain unchanged (29). In contrast, *Hip14l*$^{-/-}$ mice also showed reduced cerebellar weight that is not observed in the YAC128 HD mice. *Hip14l*$^{-/-}$ mice share some behavioural features with the YAC128 mice (Table 1). Both mice display motor learning deficits in rotarod training, motor deficits in climbing and both develop hypoactivity, albeit later in the YAC128 mice (18,31,32). Unlike the YAC128 mice, no motor coordination deficits on the rotarod task were detected in the *Hip14l*$^{-/-}$ mice (31). The normal rotarod performance of the *Hip14l*$^{-/-}$ mice may be explained by the low sensitivity of this apparatus to detect basal ganglia dysfunction (32,33). Changes in palmitoylation status of neuronal proteins are observed in both *Hip14l*$^{-/-}$ (SNAP25) and YAC128 (HIP14, HTT and GLT-1) mice (11,12,34).

Comparison of HIP14L and HIP14 protein sequence

Important functional sequences tend to be evolutionarily conserved and, as expected, this is seen in the high sequence similarity between the DHHC-CR domains of HIP14L and HIP14 (Fig. 1). The striking similarity between mouse HIP14L and HIP14 in the N-terminal half of the ankyrin domain (ANK repeats 1–3) suggests that this region may contain sequences important to some shared function between these closely related PATs. Conversely, the C-terminal half of the ankyrin

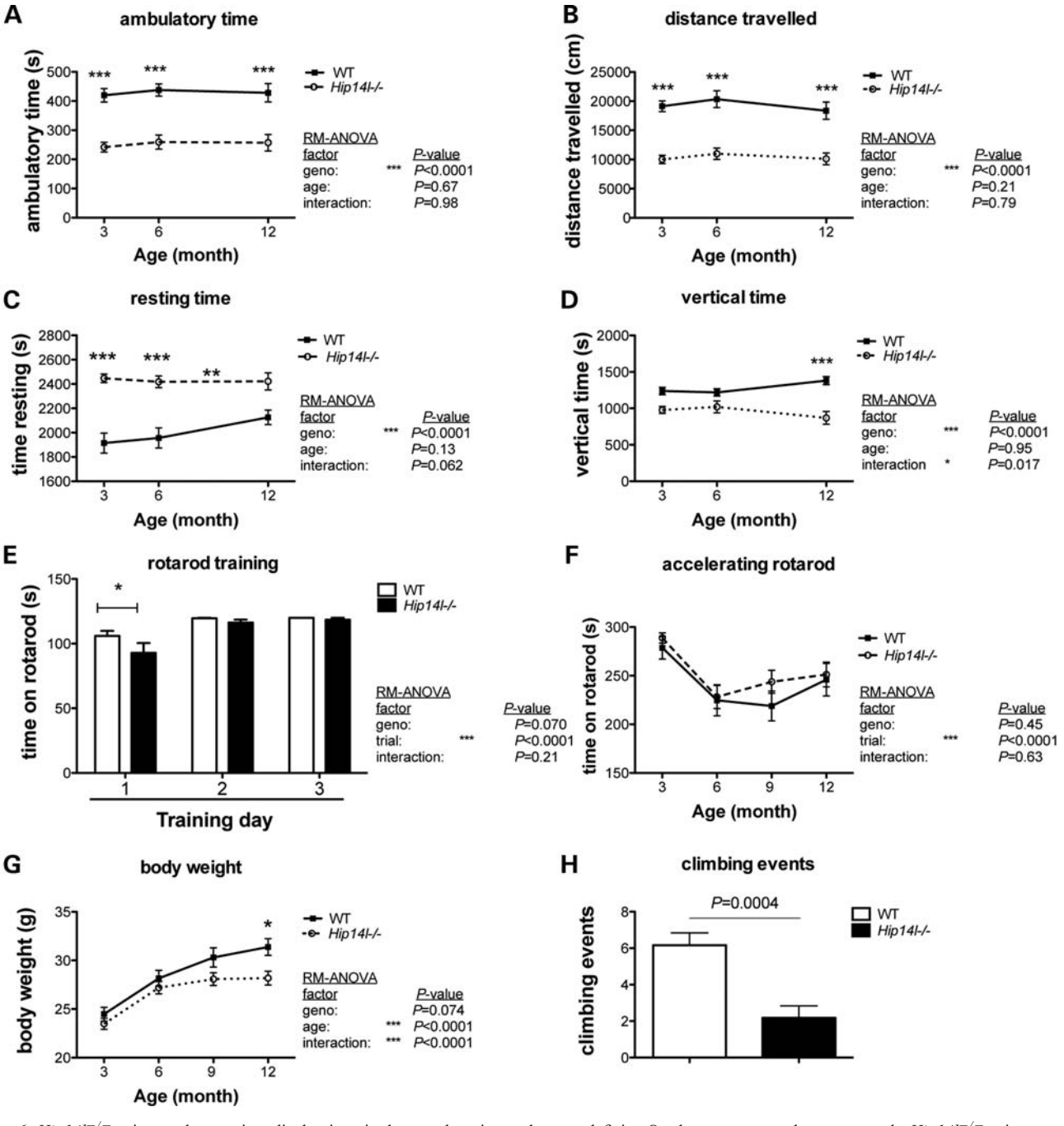

Figure 6. *Hip14l*$^{-/-}$ mice are hypoactive, display impaired motor learning and motor deficits. On the spontaneous locomotor task, *Hip14l*$^{-/-}$ mice were significantly hypoactive when compared with wild-type mice (WT) in the following measures: (**A**) ambulatory time, (**B**) distance travelled, (**C**) resting time and (**D**) vertical time. $n = 12$ (WT), $n = 9$ (*Hip14l*$^{-/-}$); mixed sex. (**E**) *Hip14l*$^{-/-}$ mice were trained for 3 days on the fixed rotarod and displayed impaired motor learning because they spent less time on the rotarod on Day 1 when compared with wild type. $n = 20$ (WT), 20 (*Hip14l*$^{-/-}$); mixed sex. (**F**) *Hip14l*$^{-/-}$ mice were tested on the accelerating rotarod task at 3, 6, 9 and 12 months of age to test motor coordination. Performance was not significantly impaired when compared with WT. $n = 15$ (WT), 18 (*Hip14l*$^{-/-}$); mixed sex. (**G**) *Hip14l*$^{-/-}$ mice displayed a trend towards reduced body weight, which is progressive. $n = 18$ (WT), 19 (*Hip14l*$^{-/-}$); mixed sex. (**H**) *Hip14l*$^{-/-}$ mice climbed less than WT mice at 2 months of age. $n = 12$ (WT), 11 (*Hip14l*$^{-/-}$). Data are represented as means $\pm$ SEM and were analyzed by RMA or Student's *t*-test. Significance of *t*-test or *post hoc* Bonferroni comparisons of genotype is indicated by *($P < 0.05$), **($P < 0.01$), ***($P < 0.001$).

domain, where the sequences diverge, is likely to confer unique functions on HIP14 and HIP14L. The critical role of the ankyrin domain of HIP14 in substrate binding has been reported previously for HTT (24,25). From limited palmitoylation substrate studies, it is apparent that HIP14L and HIP14 share some, but not all neuronal substrates (11,22). The distinct regions of high and low similarity identify segments of the ankyrin domain to be investigated for their contribution to binding shared and unique substrates of these two PATs.

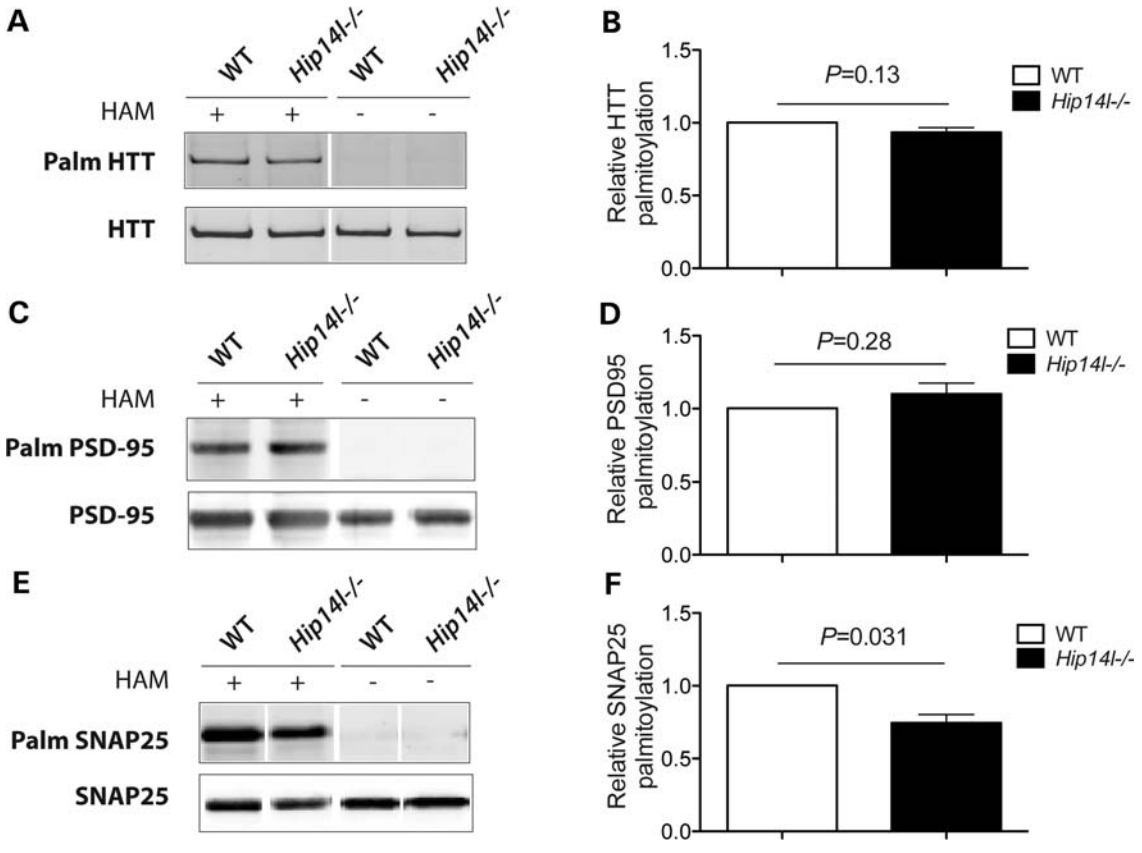

Figure 7. SNAP25 palmitoylation is reduced in *Hip14l*$^{-/-}$ brains. IP-ABE assays in *Hip14l*$^{-/-}$ whole brain at 6 weeks of age. Top panel of blots represents palmitoylated protein and the lower panel represents total immunoprecipitated protein. Hydroxylamine minus (HAM−) lanes are negative controls and represent background labelling. *Hip14l*$^{-/-}$ brain showed (**A** and **C**) no change in HTT and PSD-95 palmitoylation when compared with wild-type (WT) and (**E**) reduced SNAP25 palmitoylation. (**B**, **D**, **F**) Quantification of palmitoylation relative to immunoprecipitated protein and normalized to wild-type levels. Bars represent mean ± SEM. Data were analyzed by non-parametric Mann–Whitney test. $n = 5–6$; males.

Comparison of *Hip14l*$^{-/-}$ to *Hip14*$^{-/-}$ mice

Hip14l$^{-/-}$ mice displayed a pattern of neuropathology similar to *Hip14*$^{-/-}$ mice, but it was adult onset and progressive in manner, rather than occurring during embryonic development as in the *Hip14*$^{-/-}$ mice (Table 1). Both mouse lines show reduced brain weight and significant volume loss in striatum, cortex, globus pallidus, thalamus, cerebellum and corpus callosum and loss of enkephalin-expressing MSNs of the striatum. *Hip14*$^{-/-}$ mice display additional volume loss in the hippocampus that was not detected in the *Hip14l*$^{-/-}$ mice (11).

Hip14l$^{-/-}$ mice displayed some behavioural deficits distinct from *Hip14*$^{-/-}$ mice (Table 1). They showed hypoactivity rather than hyperactivity from 3 months of age, motor learning deficits at 3 months and no motor coordination deficits on the rotarod task from 3 to 12 months. Motor impairment was detected in the *Hip14l*$^{-/-}$ mice on the climbing task at 2 months of age, a parameter not measured in the *Hip14*$^{-/-}$ mice. As mentioned previously, the apparent absence of motor impairment in the *Hip14l*$^{-/-}$ on the accelerating rotarod task may be due to the lack of sensitivity of this apparatus to detect basal ganglia dysfunction (32,33).

Like the *Hip14*$^{-/-}$ mice, *Hip14l*$^{-/-}$ mice showed normal HTT palmitoylation in the brain (11). *In vitro* evidence indicates that HIP14 and HIP14L are the major PATs for HTT; thus, in the absence of one, the other may compensate (22). No change in *Hip14* expression was detected in *Hip14l*$^{-/-}$ brain at the transcript level (data not shown), but it may be that HIP14 compensates for the loss of HIP14L by either increased protein expression or PAT activity. Unlike *Hip14*$^{-/-}$ mice, no change in PSD-95 palmitoylation was observed in *Hip14l*$^{-/-}$ brain, which is consistent with *in vitro* observations that PSD-95 is not a HIP14L substrate (22). It still remains possible that HIP14 or another PAT might also be compensating for the loss of HIP14L in this case (11,35). SNAP25 palmitoylation was reduced in the brain of *Hip14l*$^{-/-}$ mice, like *Hip14*$^{-/-}$ mice. This deficit was present at 6 weeks of age, prior to the detection of neuropathology, suggesting that this is an upstream event that could contribute to neuronal dysfunction, rather than being a consequence of neuronal death. It is unlikely that reduced SNAP25 palmitoylation alone underlies the phenotype of the *Hip14l*$^{-/-}$ mice, but it may be that changes in palmitoylation of multiple, as yet unidentified, substrates contribute to this phenotype. SNAP25 has not previously been recognized as a HIP14L substrate because *in vitro* data only showed a mild trend ($P = 0.1$) towards a 50% increase in SNAP25 palmitoylation in the presence of HIP14L (22). This discrepancy in SNAP25 palmitoylation by HIP14L between *in vivo* and *in vitro* paradigms may reflect the fact that HIP14L is not a PAT for SNAP25 in all cellular circumstances. For example,

Table 1. Comparison of phenotypes in *Hip14l*$^{-/-}$, *Hip14*$^{-/-}$ and YAC128 HD mice

	YAC128	*Hip14*$^{-/-}$ (11)	*Hip14l*$^{-/-}$
Brain weight	5% decrease at 9 months (18) 3% decrease in volume at 3 months by MRI (29)	8% decrease at 1 month	5% decrease at 3 months
Striatal volume	5% decrease at 3 months (29)	17% decrease at E17.5 and later ages	5% decrease at 3 months
Striatal neuronal count	15% decrease at 12 months (18)	17% decrease at 1 month 17% decrease at later ages	16% decrease at 6 months
DARPP-32 and enkephalin staining	Decrease at 12 months in DARPP-32 (49)	Decrease at 1 month in DARPP-32 and enkephalin, substance P unchanged	Decrease at 6 months in DARPP-32 and enkephalin, substance P unchanged
Other brain regions affected	Decrease in volume of cortex, thalamus, globus pallidus, corpus callosum, hippocampus unchanged (29)	Decrease in volume of cortex, thalamus, globus pallidus, corpus callosum, cerebellum, hippocampus	Decrease in volume of cortex, thalamus, globus pallidus, corpus callosum, *cerebellum*, hippocampus unchanged
Motor function	Accelerating and fixed rotarod deficits from 6 months. Climbing deficits at 7 months (32). Hyperactivity at 3 months followed by hypoactivity at 6 months (18)	Accelerating and fixed rotarod deficits. Hyperactive at 3 months	*No accelerating rotarod deficits*. Climbing deficits at 2 months. Hypoactive from 3 months
Cognitive function	Impaired motor learning (31).	Normal motor learning (Young, unpublished)	Impaired motor learning
Palmitoylation	Decrease in HIP14, HTT and GLT-1 palmitoylation (11,12,34)	Decrease in PSD-95 and SNAP25 palmitoylation	Decrease in SNAP25, not PSD95, palmitoylation

Behavioural, neuropathological and palmitoylation deficits of the three mouse models. For *Hip14l*$^{-/-}$ mice, italicized text indicates how phenotype differs with YAC128 HD mice.

substrate specificity is proposed to differ between proliferating and non-proliferating cells (36). ZDHHC3, ZDHHC8 and HIP14 have all been identified as PATs for SNAP25 (22), but it is clear from the experiments here that HIP14L is an important PAT for SNAP25 in the context of the brain.

The phenotypic differences between the *Hip14l*$^{-/-}$ and *Hip14*$^{-/-}$ mice may be attributed to molecular differences of HIP14 and HIP14L, highlighted in Figure 1. As mentioned earlier, differences in substrate specificity may be due to the sequence divergence in the C-terminal half of the ankyrin domain, but other sequences or domains could also encode substrate specificity of these two PATs. Sequence variations across the two enzymes will dictate distinct interaction partners and influence the phenotypes of the PAT-deficient mice. The evolutionary differences of HIP14L and HIP14 also suggest that they have different functions. HIP14L homologs are found only in mammals, chicken and fish, and the DQHC sequence of the DHHC-CR domain is only conserved in mammals. In contrast, HIP14 is conserved down to yeast (7). This suggests that HIP14L may have evolved a function in vertebrates unique to its functions shared with HIP14, which may include its role in hair follicle development.

HIP14 and HIP14L are reported to possess other non-PAT functions. HIP14 and HIP14L activate the JNK pathway (37). Like the yeast homolog of Hip14, Akr1, that can suppress the yeast pheromone pathway independently of its PAT activity (38), HIP14 regulates the JNK pathway independently of its PAT activity (39). HIP14 and HIP14L are also magnesium transporters (40). Loss of these non-PAT functions may also contribute to the phenotypes observed in the *Hip14*- and *Hip14l*-deficient mice.

Contribution of HIP14L and HIP14 to the pathogenesis of HD

The adult-onset, progressive neuropathology, motor deficits and palmitoylation deficits of the *Hip14l*$^{-/-}$ mouse are highly reminiscent of the YAC128 HD mouse model and human HD (16,18). HTT palmitoylation is reduced in the YAC128 mice, but unchanged in *Hip14*- and *Hip14l*-deficient mice (11,12), suggesting that both HIP14 and HIP14L may be dysfunctional in HD. Thus, reduced HIP14- and HIP14L-dependent palmitoylation of neuronal substrates may underlie some of the features of HD, strongly supporting the concept that aberrant palmitoylation contributes to neuropsychiatric diseases.

Comparison of *Hip14l*$^{-/-}$ and *Hip14l*^{R425X} mutant mice

The phenotypes observed in this study for the *Hip14l*$^{-/-}$ mice do not match those reported by Saleem *et al.* for the *Hip14l*^{R425X} mutant mice, which included deficits in survival, body weight, hair, skin and bone and generalized amyloidosis (26). In contrast to the *Hip14l*^{R425X} mice that were reported to carry a loss of function allele, *Hip14l*$^{-/-}$ mice did not display reduced survival, skeletal deficits or amyloid deposition. The *Hip14l*$^{-/-}$ mice did develop hair pathology (periocular alopecia) and 10% reduced body weight at 12 months of age (Fig. 6G), but these phenotypes were much milder than the severe alopecia and 50% reduced body weight reported for

the *Hip14l*^{R425X} mice. The authors stated that a *Hip14l* gene trap mouse (generated with the identical construct used in our study) exhibited the same phenotypes as the *Hip14l*^{R425X} mice, but unfortunately only skin histology data were presented, making it difficult to compare it with the *Hip14l*$^{-/-}$ data presented here.

The background strain is known to modulate the severity of phenotypes in mice; thus, the phenotypic differences observed in these two studies may be strain related (41–43). The *Hip14l*^{R425X} and *Hip14l* gene trap mutants in Saleem *et al.* were on a BL/6 × 129 mixed background and our *Hip14l* $^{-/-}$ mice were on an FVB background.

The *Hip14l*^{R425X} mouse contains a nonsense mutation located in exon 12 of the *Hip14l* gene. This mutation is predicted to truncate the protein at residue 425 (hence R425X), just prior to the DHHC-CR catalytic domain (aa426–476) and accordingly abolishes the enzymatic activity. The ankyrin domain and the first four transmembrane domains are retained, suggesting that the truncated protein should be membrane bound. The ankyrin and DHHC-CR domains of Akr1, the yeast homolog of HIP14 and HIP14L, are able to carry out Akr1 function, even when expressed from separate mRNAs, provided they are membrane tethered (38). Thus, it is possible that rather than leading to loss of function, HIP14L^{R425X} is acting in a dominant-negative manner. HIP14L^{R425X} may bind substrates, but would be unable to palmitoylate them, leading to their mislocalization. By sequestering substrates, HIP14L^{R425X} may also prevent HIP14, and possibly even other PATS, from compensating and palmitoylating those substrates (22,44). This dominant-negative function of HIP14L^{R425X} and lack of compensation by other PATs would be expected to result in an exacerbated phenotype as compared to the loss of HIP14L function alone.

The *Hip14l*$^{-/-}$ mouse described herein lacks any *Hip14l* mRNA expression and is therefore a genuine model of complete *Hip14l* deficiency. A mouse model with a potential dominant-negative mutation does not represent a mouse model with complete deletion of HIP14L function. Thus, our model unambiguously represents the biochemical, neuropathological, behavioural and pathological phenotypes resulting from the absence of HIP14L.

MATERIALS AND METHODS

HIP14L and HIP14 sequence comparison

The conservation plot was generated by EMBOSS Plotcon (45) with a window size of 50 amino acids and other parameters at default values using a sequence alignment of mouse HIP14L (NP_082307.1) and HIP14 (NP_766142.2) as input. The Plotcon similarity score is calculated from the pairwise amino acid substitution score from the EBLOSUM62 substitution matrix as a factor of window size and number of sequences compared and was normalized to a maximum of 1.

Antibodies

The antibodies used in this study were HTT rabbit polyclonal antibody [BKP1 (46); 1:30 for immunoprecipitation (IP)], HTT mouse monoclonal antibody (MAB2166, Millipore, 1:1000 for IP), GFP goat polyclonal antibody (G095, Applied Biological Materials, 1:100 for IP), GFP rabbit polyclonal antibody (sc8334, Santa Cruz, 1:200 for immunoblotting), SNAP25 mouse monoclonal (SMI81, Covance, 1:125 for IP), SNAP25 rabbit polyclonal (111002, Synaptic Systems, 1:1000 for immunoblotting), PSD-95 rabbit polyclonal (in-house, 1:85 for IP) and PSD-95 mouse monoclonal (MA1-25629, Thermoscientific, 1:1000 for immunoblotting). Fluorescently conjugated secondary antibodies for immunoblotting were streptavidin Alexa Fluor 680 conjugate (1:10 000, Invitrogen), Alexa Fluor 680 donkey anti-mouse antibody (1:10 000, Invitrogen) and goat anti-mouse and goat anti-rabbit IRDye800CW conjugate antibodies (1:10 000; Rockland, Gilbertsville, PA, USA).

Cell culture and transfection

All reagents for cell culture were purchased from Invitrogen unless stated otherwise. Human N548-HTT in pCIneo, either wild type (15Q) or mutant (128Q), were co-transfected in COS-7 cells with either human HIP14L-GFP in pCIneo or human HIP14-GFP in pCIneo (23) using FuGENE6 (Roche), according to the manufacturer's instructions. Cells were harvested after 24 h for co-IP experiments described below.

Cell lysis and co-IP

Cells were homogenized on ice in one volume 1%SDS/TEEN [TEEN: 50 mM Tris pH 7.5, 1 mM EDTA, 1 mM EGTA, 150 mM NaCl, 1× Complete protease inhibitor cocktail (Roche), 200 mM sodium vanadate, 200 mM PMSF and 5 mM zVAD) prior to dilution in four volumes 1% TritonX-100/TEEN for further homogenization and incubation for 5 min on ice. Samples were sonicated to shear DNA, and the insoluble material was removed by centrifugation at 14 000 revolution per minute (rpm) for 15 min. Samples were immunoprecipitated with protein G sepharose beads (GE Healthcare) and goat polyclonal GFP antibody (see the Antibodies section).

Immunoblotting

Proteins in both the cell lysates and immunoprecipitates were heated at 70°C in 1× NuPAGE LDS sample buffer (Invitrogen) with 10 mM DTT for co-IPs and 100 mM DTT for palmitoylation assays before separation by SDS-PAGE. After transfer of the proteins onto nitrocellulose membranes or Immobilon-PVDF-FL membrane (for co-IPs), immunoblots were performed using the indicated primary antibody and the corresponding secondary antibody as described in the Antibodies section. Fluorescence was scanned and quantified with Odyssey Infrared Imaging system (Li-COR Bioscience) as described in (25). Odyssey Infrared imaging offers a very wide quantitative linear range, and all fluorescence signals used for quantitation were within the linear range of detection.

Generation of *Hip14l*-deficient mice

AC0492 embryonic stem cells (E14Tg2a.4; from parental line 129P2/OlaHsd) harbouring a gene trap vector in intron 1 of

the *Hip14l* gene (*Zdhhc13*) were purchased from BayGenomics and microinjected into C57BL/6 mice (BayGenomics database http://www.genetrap.org/). Chimeric mice were backcrossed with FVB/NJ mice for five generations (N5). Mice were genotyped by PCR with primers flanking the 5′ integration site: a common forward primer within the endogenous gene (5′- CTCCCAGTCTTGGTCTTCACTAC-3′) and a reverse primer specific to the gene trap vector (pGT0lxr; 5′-GAACTTCCCTAGGCCTATCAC-3′) and to the endogenous gene (5′- GAGCAAGCGCATCATCAGGATC-3′), resulting in PCR products of 374 bp for the mutant allele and 680 bp for the wild-type allele. All animal procedures were approved by the University of British Columbia Committee on Animal Care (protocol numbers A07-0106 and A12-0063).

Quantitative PCR (qRT-PCR)

Total RNA was extracted from dissected tissue, frozen and stored at −80°C using the RNAeasy mini kit (Qiagen, 74104). RNA was treated with DNAse I (Invitrogen) to remove residual genomic DNA. cDNA was generated using the SuperScript® III First-Strand Synthesis System (Invitrogen) from 1 μg RNA with oligo-dT primers. Mouse *Hip14l* primers were obtained from Primerbank (http://pga.mgh.harvard.edu/primerbank/index.html) and were located in exon 4 and 5: *Hip14l* forward: 5′-TGGGTGGTGACCTAAATTCAACT-3′ and reverse: 5′-GCACCGTGCTGGAGCAATA-3′. Mouse actin forward: 5′- ACGGCCAGGTCATCACTATTG-3′ and reverse: 5′- CAAGAAGGAAGGCTGGAAAAGA-3′. qRT-PCR was performed using *Power* SYBR Green PCR master mix (Applied Biosystems, 4367659) in the ABI 7500 instrument (Applied Biosystems). The relative gene expression, normalized to mouse actin, was calculated using the $\Delta\Delta C_T$ method.

Neuropathology

Neuropathological assessments for brain and cerebellar weights, striatal and cortical volumes and striatal neuron number were conducted as previously reported (18), with the tester blind to the genotype. DARPP-32 and enkephalin staining and quantification were performed as described in (11). Corpus callosum volume was determined in every eighth NeuN-stained section from Bregma 1.18 mm to −0.94 mm with cortex and striatum as dorsal and ventral boundaries. The hippocampal volume was determined in every eighth NeuN-stained section, spanning from Bregma −0.94 mm to −2.8 mm. The globus pallidus volume was determined in every eighth NeuN-stained section, spanning from bregma 0.02 mm to −1.7 mm with the internal capsule as the medial boundary, striatum as the lateral boundary and an imaginary line from the anterior commissure to the internal capsule was used as the ventral boundary. The thalamus volume was determined in every eighth NeuN-stained section from Bregma −0.94 to −2.54 mm as previously described (47). Volumes were calculated using the Cavalieri principle.

Behaviour analysis

All behaviour testing was performed with the tester blind to the genotype.

Accelerating rotarod was used to assess the motor coordination (UGO Basile, Comerio, Italy) as previously described (18). Mice were trained during three 120 s trials daily for three consecutive days on a fixed 18 rpm rotarod. Latency to the first fall and number of falls per trail were scored, and the average of the three trials was reported. For longitudinal rotarod performance, mice were tested on a rotarod accelerating from 5 to 40 rpm over 300 s. Latency to fall was scored, and the average of three trials was reported.

Spontaneous activity was assessed using the Med Associates activity monitor system (Med Associates Inc., St Albans, VT, USA) as described in (11). Mice were given transgel (Charles River) and acclimatized to the room for at least 1 h prior to testing, and the testing did not commence until 1 h after the beginning of the dark cycle. The chamber was cleaned with ethanol and allowed to dry between each animal. Each mouse was placed in the centre of the testing chamber. A number of automated readouts were recorded for 60 min, binned at 5 min intervals.

Climbing was assessed as previously described (32). Briefly, mice were placed in a closed-top wire mesh cylinder (10 × 15 cm) on the tabletop, and spontaneous activity was recorded with a video camera for 5 min. The time from when a mouse's fourth foot left the table top to the time when the first foot was replaced on the table top was scored as time spent climbing and as a climbing event. The sum of climbing time, number of climbing events, latency to climb and number of rearing events in the 5 min trial was scored.

IP-acyl-biotin exchange (ABE) palmitoylation assay

Brains were harvested and immediately snap-frozen in liquid nitrogen and then stored at −80°C. In brief, frozen half brains were homogenized into 5 ml lysis buffer (150 mM NaCl, 50 mM Tris, 5 mM ethylenediaminetetraacetic acid, pH 7.4) with 50 mM *N*-ethylmaleimide (NEM). Proteins of interest were immunoprecipitated from lysates (250–500 μl) overnight with Protein G Dynabeads (Invitrogen) using specific antibodies (as listed above). Acyl-biotin exchange (ABE) chemistry was applied as described in (22,48). Male brains were used at 6 weeks of age for $Hip14l^{-/-}$ and wild-type littermate controls. Data were analyzed using the Wilcoxon matched pair non-parametric test.

SUPPLEMENTARY MATERIAL

Supplementary Material is available at *HMG* online.

ACKNOWLEDGEMENTS

The authors would like to thank Nagat Bissada, Tess Lengyell, Amanda Spreeuw, Mark Wang and the Histology Core Lab (Child and Family Research Institute, Vancouver, BC) for technical assistance, Dr Kevin McElwee (UBC) for advice on hair follicle experiments and Dr Dale Martin for advice on the manuscript.

Conflict of Interest statement. None declared

FUNDING

This work was supported by the Canadian Institutes of Health Research (www.cihr-irsc.gc.ca; operating grant number GPG-102165 to M.R.H., and a Doctoral Research Award to S.S.S.); Michael Smith Foundation for Health Research (www.msfhr.org; Junior Graduate Scholarship to S.S.S. and post-doctoral fellowship to R.R.S.); Ripples of Hope Pfizer (2011 Trainee Award in Rare Diseases to L.M.S.) and CHDI Foundation, Inc. (chdifoundation.org; operating grant to M.R.H.). The funders had no role in study design and analysis, decision to publish or preparation of the manuscript.

REFERENCES

1. Fukata, Y. and Fukata, M. (2010) Protein palmitoylation in neuronal development and synaptic plasticity. *Nat. Rev. Neurosci.*, **11**, 161–175.
2. Kanaani, J., El-Husseini, A.E., Aguilera-Moreno, A., Diacovo, J.M., Bredt, D.S. and Baekkeskov, S. (2002) A combination of three distinct trafficking signals mediates axonal targeting and presynaptic clustering of GAD65. *J. Cell Biol.*, **158**, 1229–1238.
3. Kanaani, J., Diacovo, M.J., El-Husseini, A.E., Bredt, D.S. and Baekkeskov, S. (2004) Palmitoylation controls trafficking of GAD65 from Golgi membranes to axon-specific endosomes and a Rab5a-dependent pathway to presynaptic clusters. *J. Cell Sci.*, **117**, 2001–2013.
4. Craven, S.E., El-Husseini, A.E. and Bredt, D.S. (1999) Synaptic targeting of the postsynaptic density protein PSD-95 mediated by lipid and protein motifs. *Neuron*, **22**, 497–509.
5. Ehrlich, I. and Malinow, R. (2004) Postsynaptic density 95 controls AMPA receptor incorporation during long-term potentiation and experience-driven synaptic plasticity. *J. Neurosci.*, **24**, 916–927.
6. El-Husseini, A.E., Craven, S.E., Chetkovich, D.M., Firestein, B.L., Schnell, E., Aoki, C. and Bredt, D.S. (2000) Dual palmitoylation of Psd-95 mediates its vesiculotubular sorting, postsynaptic targeting, and ion channel clustering. *J. Cell Biol.*, **148**, 159–172.
7. Young, F.B., Butland, S.L., Sanders, S.S., Sutton, L.M. and Hayden, M.R. (2012) Putting proteins in their place: palmitoylation in Huntington disease and other neuropsychiatric diseases. *Prog. Neurobiol.*, **97**, 220–238.
8. Liu, H., Abecasis, G.R., Heath, S.C., Knowles, A., Demars, S., Chen, Y-J., Roos, J.L., Rapoport, J.L., Gogos, J.A. and Karayiorgou, M. (2002) Genetic variation in the 22q11 locus and susceptibility to schizophrenia. *Proc. Natl. Acad. Sci. USA*, **99**, 16859–16864.
9. Mukai, J., Liu, H., Burt, R.A., Swor, D.E., Lai, W.-S., Karayiorgou, M. and Gogos, J.A. (2004) Evidence that the gene encoding ZDHHC8 contributes to the risk of schizophrenia. *Nat. Genet.*, **36**, 725–731.
10. Mukai, J., Dhilla, A., Drew, L.J., Stark, K.L., Cao, L., MacDermott, A.B., Karayiorgou, M. and Gogos, J.A. (2008) Palmitoylation-dependent neurodevelopmental deficits in a mouse model of 22q11 microdeletion. *Nat. Neurosci.*, **11**, 1302–1310.
11. Singaraja, R.R., Huang, K., Sanders, S.S., Milnerwood, A.J., Hines, R., Lerch, J.P., Franciosi, S., Drisdel, R.C., Vaid, K., Young, F.B. *et al.* (2011) Altered palmitoylation and neuropathological deficits in mice lacking HIP14. *Hum. Mol. Genet.*, **20**, 3899–3909.
12. Yanai, A., Huang, K., Kang, R., Singaraja, R.R., Arstikaitis, P., Gan, L., Orban, P.C., Mullard, A., Cowan, C.M., Raymond, L.A. *et al.* (2006) Palmitoylation of huntingtin by HIP14 is essential for its trafficking and function. *Nat. Neurosci.*, **9**, 824–831.
13. Mizumaru, C., Saito, Y., Ishikawa, T., Yoshida, T., Yamamoto, T., Nakaya, T. and Suzuki, T. (2009) Suppression of APP-containing vesicle trafficking and production of β-amyloid by AID/DHHC-12 protein. *J. Neurochem.*, **111**, 1213–1224.
14. Vesa, J., Hellsten, E., Verkruyse, L.A., Camp, L.A., Rapola, J., Santavuori, P., Hofmann, S.L. and Peltonen, L. (1995) Mutations in the palmitoyl protein thioesterase gene cause infantile neuronal ceroid lipofuscinosis. *Nature*, **376**, 584–587.
15. Raymond, F., Tarpey, P.S., Edkins, S., Tofts, C., O'Meara, S., Teague, J., Butler, A., Stevens, C., Barthorpe, S., Buck, G. *et al.* (2007) Mutations in ZDHHC9, which encodes a palmitoyltransferase of NRAS and HRAS, cause x-linked mental retardation associated with a marfanoid habitus. *Am. J. Hum Genet.*, **80**, 982–987.
16. Vonsattel, J.P. and DiFiglia, M. (1998) Huntington disease. *J. Neuropathol. Exp. Neurol.*, **57**, 369–384.
17. The Huntington's Disease Collaborative Research Group (1993) A novel gene containing a trinucleotide repeat that is expanded and unstable on Huntington's disease chromosomes. *Cell*, **72**, 971–983.
18. Slow, E.J., Van Raamsdonk, J., Rogers, D., Coleman, S.H., Graham, R.K., Deng, Y., Oh, R., Bissada, N., Hossain, S.M. and Yang, Y. (2003) Selective striatal neuronal loss in a YAC128 mouse model of Huntington disease. *Hum. Mol. Genet.*, **12**, 1555–1567.
19. Roth, A.F., Feng, Y., Chen, L. and Davis, N.G. (2002) The yeast DHHC cysteine-rich domain protein Akr1p is a palmitoyl transferase. *J. Cell Biol.*, **159**, 23–28.
20. Linder, M.E. and Deschenes, R.J. (2007) Palmitoylation: policing protein stability and traffic. *Nat. Rev. Mol. Cell Biol.*, **8**, 74–84.
21. Ohno, Y., Kihara, A., Sano, T. and Igarashi, Y. (2006) Intracellular localization and tissue-specific distribution of human and yeast DHHC cysteine-rich domain-containing proteins. *Biochim. Biophys. Acta*, **1761**, 474–483.
22. Huang, K., Sanders, S., Singaraja, R., Orban, P., Cijsouw, T., Arstikaitis, P., Yanai, A., Hayden, M.R. and El-Husseini, A. (2009) Neuronal palmitoyl acyl transferases exhibit distinct substrate specificity. *FASEB J.*, **23**, 2605–2615.
23. Huang, K., Yanai, A., Kang, R., Arstikaitis, P., Singaraja, R.R., Metzler, M., Mullard, A., Haigh, B., Gauthier-Campbell, C., Gutekunst, C.-A. *et al.* (2004) Huntingtin-interacting protein HIP14 is a palmitoyl transferase involved in palmitoylation and trafficking of multiple neuronal proteins. *Neuron*, **44**, 977–986.
24. Singaraja, R.R., Hadano, S., Metzler, M., Givan, S., Wellington, C.L., Warby, S., Yanai, A., Gutekunst, C-A., Leavitt, B.R., Yi, H. *et al.* (2002) HIP14, a novel ankyrin domain-containing protein links huntingtin to intracellular trafficking and endocytosis. *Hum. Mol. Genet.*, **11**, 2815–2828.
25. Huang, K., Sanders, S.S., Kang, R., Carroll, J.B., Sutton, L., Wan, J., Singaraja, R., Young, F.B., Liu, L., El-Husseini, A. *et al.* (2011) Wild-type HTT modulates the enzymatic activity of the neuronal palmitoyl transferase HIP14. *Hum. Mol. Genet*, **20**, 3356–3365.
26. Saleem, A.N., Chen, Y.-H., Baek, H.J., Hsiao, Y.-W., Huang, H.-W., Kao, H.-J., Liu, K.-M., Shen, L.-F., Song, I.-W., Tu, C.-P.D. *et al.* (2010) Mice with alopecia, osteoporosis, and systemic amyloidosis due to mutation in Zdhhc13, a gene coding for palmitoyl acyltransferase. *PLoS Genet.*, **6**, e1000985.
27. Fairbank, M., Huang, K., El-Husseini, A. and Nabi, I.R. (2012) RING finger palmitoylation of the endoplasmic reticulum Gp78 E3 ubiquitin ligase. *FEBS Lett.*, **586**, 2488–2493.
28. Alonso, L. and Fuchs, E. (2006) The hair cycle. *J. Cell Sci.*, **119**, 391–393.
29. Carroll, J.B., Lerch, J.P., Franciosi, S., Spreeuw, A., Bissada, N., Henkelman, R.M. and Hayden, M.R. (2011) Natural history of disease in the YAC128 mouse reveals a discrete signature of pathology in Huntington disease. *Neurobiol. Dis.*, **43**, 257–265.
30. Deng, Y., Albin, R.L., Penney, J.B., Young, A.B., Anderson, K.D. and Reiner, A. (2004) Differential loss of striatal projection systems in Huntington's disease: a quantitative immunohistochemical study. *J. Chem. Neuroanat.*, **27**, 143–164.
31. Van Raamsdonk, J.M., Pearson, J., Slow, E.J., Hossain, S., Leavitt, B.R. and Hayden, M.R. (2005) Cognitive dysfunction precedes neuropathology and motor abnormalities in the YAC128 mouse model of Huntington's disease. *J. Neurosci.*, **25**, 4169–4180.
32. Southwell, A.L., Ko, J. and Patterson, P.H. (2009) Intrabody gene therapy ameliorates motor, cognitive, and neuropathological symptoms in multiple mouse models of Huntington's disease. *J. Neurosci.*, **29**, 13589–13602.
33. Hickey, M.A., Kosmalska, A., Enayati, J., Cohen, R., Zeitlin, S., Levine, M.S. and Chesselet, M.-F. (2008) Extensive early motor and non-motor behavioral deficits are followed by striatal neuronal loss in knock-in Huntington's disease mice. *Neuroscience*, **157**, 280–295.
34. Huang, K., Kang, M.H., Askew, C., Kang, R., Sanders, S.S., Wan, J., Davis, N.G. and Hayden, M.R. (2010) Palmitoylation and function of glial glutamate transporter-1 is reduced in the YAC128 mouse model of Huntington disease. *Neurobiol. Dis.*, **20**, 207–215.
35. Fukata, M., Fukata, Y., Adesnik, H., Nicoll, R.A. and Bredt, D.S. (2004) Identification of PSD-95 palmitoylating enzymes. *Neuron*, **44**, 987–996.

36. Mitchell, D.A., Vasudevan, A., Linder, M.E. and Deschenes, R.J. (2006) Protein palmitoylation by a family of DHHC protein S-acyltransferases. *J. Lipid Res.*, **47**, 1118–1127.
37. Harada, T., Matsuzaki, O., Hayashi, H., Sugano, S., Matsuda, A. and Nishida, E. (2003) AKRL1 and AKRL2 activate the JNK pathway. *Genes Cells*, **8**, 493–500.
38. Hemsley, P.A. and Grierson, C.S. (2011) The ankyrin repeats and DHHC S-acyl transferase domain of AKR1 act independently to regulate switching from vegetative to mating states in yeast. *PLoS One*, **6**, e28799.
39. Yang, G. and Cynader, M.S. (2011) Palmitoyl acyltransferase zD17 mediates neuronal responses in acute ischemic brain injury by regulating JNK activation in a signaling module. *J. Neurosci.*, **31**, 11980–11991.
40. Goytain, A., Hines, R.M. and Quamme, G.A. (2008) Huntingtin-interacting proteins, HIP14 and HIP14L, mediate dual functions, palmitoyl acyltransferase and mg^{2+} transport. *J. Biol. Chem.*, **283**, 33365–33374.
41. Holmes, A., Lit, Q., Murphy, D.L., Gold, E. and Crawley, J.N. (2003) Abnormal anxiety-related behavior in serotonin transporter null mutant mice: the influence of genetic background. *Genes Brain Behav.*, **2**, 365–380.
42. Houde, C., Banks, K.G., Coulombe, N., Rasper, D., Grimm, E., Roy, S., Simpson, E.M. and Nicholson, D.W. (2004) Caspase-7 expanded function and intrinsic expression level underlies strain-specific brain phenotype of caspase-3-null mice. *J. Neurosci.*, **24**, 9977–9984.
43. Peinado, J.R., Laurent, V., Lee, S., Peng, B.W., Pintar, J.E., Steiner, D.F. and Lindberg, I. (2005) Strain-dependent influences on the hypothalamo-pituitary-adrenal axis profoundly affect the 7B2 and PC2 null phenotypes. *Endocrinology*, **146**, 3438–3444.
44. Greaves, J. and Chamberlain, L.H. (2011) DHHC palmitoyl transferases: substrate interactions and (patho)physiology. *Trends in Biochem. Sci.*, **36**, 245–253.
45. Rice, P., Longden, I. and Bleasby, A. (2000) The European molecular biology open software suite. *Trends in Genet.*, **16**, 276–277.
46. Wellington, C.L., Ellerby, L.M., Gutekunst, C.-A., Rogers, D., Warby, S., Graham, R.K., Loubser, O., van Raamsdonk, J., Singaraja, R., Yang, Y.-Z. *et al.* (2002) Caspase cleavage of mutant huntingtin precedes neurodegeneration in Huntington's disease. *J. Neurosci.*, **22**, 7862–7872.
47. Christensen, D.Z., Kraus, S.L., Flohr, A., Cotel, M.-C., Wirths, O. and Bayer, T.A. (2008) Transient intraneuronal Aβ rather than extracellular plaque pathology correlates with neuron loss in the frontal cortex of APP/PS1KI mice. *Acta Neuropathol*, **116**, 647–655.
48. Drisdel, R.C. and Green, W.N. (2004) Labeling and quantifying sites of protein palmitoylation. *BioTechniques*, **36**, 276–285.
49. Van Raamsdonk, J.M., Pearson, J., Rogers, D.A., Lu, G., Barakauskas, V.E., Barr, A.M., Honer, W.G., Hayden, M.R. and Leavitt, B.R. (2005) Ethyl-EPA treatment improves motor dysfunction, but not neurodegeneration in the YAC128 mouse model of Huntington disease. *Exp. Neurol.*, **196**, 266–272.